Nanoscale avalanche photodiode with self-quenching and ultrahigh ultraviolet/visible rejection ratio

Rongdun Hong,[1] Yi Zhou,[3] Yannan Xie,[1] Xiaping Chen,[1] Zifeng Zhang,[1] Kang L. Wang,[2] and Zhengyun Wu[1,*]

[1]*Physics and Mechanical & Electrical Engineering School, Xiamen University, Xiamen, 361005 Fujian, China*

[2]*Electrical Engineering Department, University of California, Los Angeles, California 90095, USA*

[3]*Applied Materials, Inc., 974 East Arques Avenue, Sunnyvale, California 94085, USA*

**Corresponding author: zhywu@xmu.edu.cn*

Received May 21, 2012; revised July 19, 2012; accepted July 19, 2012;
posted July 30, 2012 (Doc. ID 169028); published August 28, 2012

A 4H-SiC based separate-absorption-multiplication (SAM) avalanche photodiode with a nanoscale multiplication region and a bulk absorption region is proposed and its optoelectronic performance is modeled. The results show that the avalanche breakdown voltage of the device is found to be dependent on the illumination condition. This is attributed to the existence of an illumination-dependent hole potential well in the upper center of the absorption region. Based on the illumination-dependence of avalanche breakdown voltage, a self-quenching and an ultrahigh UV/visible rejection ratio have been realized in this structure. © 2012 Optical Society of America

OCIS codes: 040.0040, 040.1345, 040.5160, 040.7190.

Currently, photomultiplier tubes (PMTs) are widely used for the detection of light at ultraviolet (UV) wavelengths. Nevertheless, PMTs are typically bulky, fragile, and expensive, which leaves a space for developing alternative devices for the UV-light detection. Due to material merits including wide band-gap, high critical field, high carrier saturation velocity, and high thermal conductivity, certain semiconductor material systems including SiC, ZnO, GaN, and TiO_2 have attracted research interest recently as a replacement for PMTs. One application of particular interest is high power, high frequency, optoelectronic devices [1–4].

In the past two decades, worldwide efforts in nanomaterials research has led to a rich collection of nanostructures where size, shape, and composition can be readily controlled. Many such nanostructures exhibit fascinating optical properties that could have significant impact in the future for photonic technology [5]. In recent years, nanostructures that efficiently detect optical inputs and process them into electrical outputs have attracted considerable interest for improving the electro-optical properties of bulk photodiodes. Several nanoscale photodiodes have been reported [6–8].

The avalanche photodiode (APD) currently dominates the research field of the weak signal and single photon UV detection. This is due principally to the signal-to-noise ratio enhancement provided by the internal carrier multiplication process that characterizes these devices [9]. Several wide band-gap semiconductor materials including 4H-SiC (~3.2 eV) [10] and GaN (~3.4 eV) [11] are not completely solar-blind as photons having wavelengths longer than 285 nm [12] can promote carriers in these material systems. This can result in a low UV/visible rejection ratio. Filters are sometimes used to enhance the rejection of solar wavelengths [13].

Therefore, in this Letter, an APD with a large bulk absorption region and a nanoscale avalanche region (NAPD) is proposed. The NAPD can be regarded as a nanoscale separate-absorption-multiplication (SAM) APD. Provided the scale of the avalanche region is small enough, the electric field inside the vertical SAM-APD can interact with the electric field of the lateral P^+N^- diode such that the NAPD's breakdown voltage (V_{br}) is modified. The illumination-dependent V_{br} of the NAPD would result in self-quenching characteristic and an ultra-high UV/visible rejection ratio for the device. 4H-SiC is selected as the material in this work for the simulation of the NAPD's optoelectronic characteristics, as the 4H-SiC APDs have been well studied in recent years [14–16].

By employing the physical models and material parameters reported by Cha's and Sandvik [17], the device modeling was done using the ATLAS software package from SILVACO. Figure 1(a) shows the typical device structure of the 4H-SiC NAPD used for this modeling, which features a large bulk absorption region underneath a nanoscale pillar, built on an N^+-type substrate. The diameter of the nanoscale pillar is 200 nm and the entire

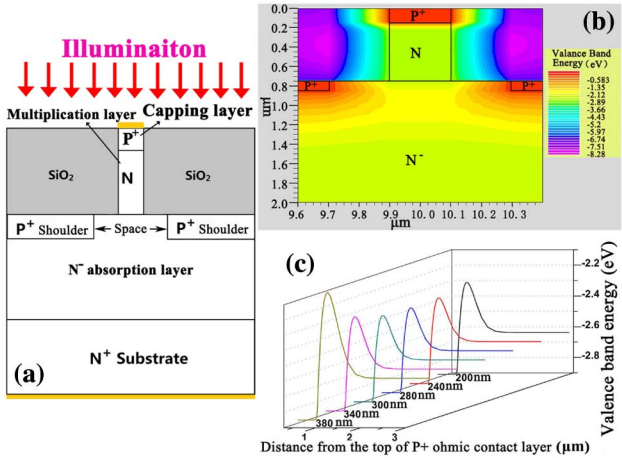

Fig. 1. (Color online) (a) Typical structure of the 4H-SiC NAPD, (b) the valence band contour distribution of the 4H-SiC NAPD without illumination and bias, and (c) the valence band diagrams of the 4H-SiC NAPD at the center of the device as a function of the distance from the top of P^+ capping layer, in which the operation voltage is 0 V and P is 1×10^{-4} W/cm^2.

device is 20.0 μm wide. The pillar, located at the device's upper center, contains a 0.6 μm thick N-type multiplication region and a 0.15 μm thick P^+-type capping layer. The absorption region contains a 9.0 μm thick N^--type layer and a 100 nm thick P^+-type shoulders. The P^+-type shoulders, with a space of 0.6 μm in the N^--type region, can not only provide a depletion region for the absorption of photons, but also provide an electric field of the lateral P^+N^- diode interacting with the electric field inside the vertical SAM-APD to modify the breakdwon voltage. Then, a 0.8 μm thick SiO_2 layer is designed as the passivation layer above the absorption region and surrounding the pillar. The doping level for P^+ capping, N, P^+ shoulder, N^- and N^+ layers are $3.0 \times 10^{19}/cm^3$, $4.0 \times 10^{17}/cm^3$, $3.0 \times 10^{19}/cm^3$, $3.0 \times 10^{15}/cm^3$, and $1.0 \times 10^{19}/cm^3$, respectively. During the modeling, the illumination is vertically incident on the device and uniformly covers the whole upper surface of the device.

Figure 2 shows the dependence of the 4H-SiC NAPD's V_{br} on illumination wavelength (λ), where the illumination power density (P) is 1×10^{-4} W/cm^2. The Fig. 2 inset shows the dependence of V_{br} on incident optical power at 280 nm. It is noted that, as λ increases from 200 to 400 nm, V_{br} first falls until λ is around 300 nm, and then increases with λ. Moreover, while P drops from 1×10^{-2} W/cm^2 to 0 W/cm^2, the V_{br} increases gradually to a saturation value. It is the nanoscale structure of the NAPD that accounts for the characteristic of illumination-dependent V_{br}, which will be demonstrated as follows.

The valence band contour distribution of the 4H-SiC NAPD without illumination and bias is illustrated in Fig. 1(b). The valence band contour distribution shows that the electron energy in the upper center of the N^- region is higher than that in the pillar region and the bottom N^- region, which will restrict the vertical drift of the holes. The valence band diagrams of the 4H-SiC NAPD at the center of the device as a function of the distance from the top of P^+ capping layer are illustrated in Fig. 1(c), in which the operation voltage is 0 V and P is 1×10^{-4} W/cm^2. As λ increases from 200 to 380 nm, there are hole potential wells in all the valence band diagrams

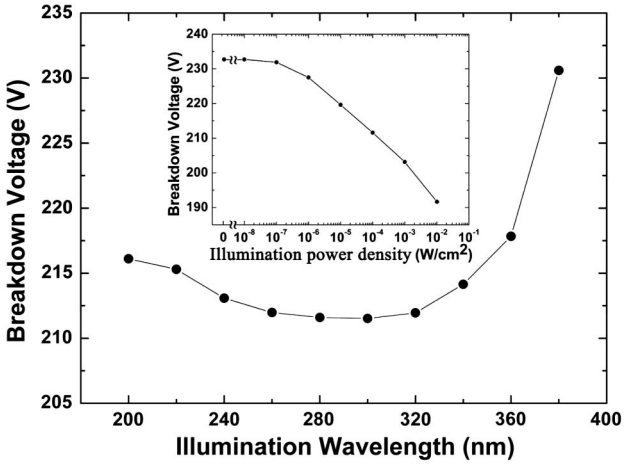

Fig. 2. Dependence of 4H-SiC NAPD's breakdown voltage (V_{br}) on the wavelength (λ) where the illumination power density is 1×10^{-4} W/cm^2, and the dependence of V_{br} on incident optical power at 280 nm (Inset).

and the depth of the hole potential well decreases first until λ is 280 nm, then increases with λ. The existence of the hole potential well is due to the P^+ shoulders of the device. Assuming the space between the P^+ shoulders is small enough, the N^- region in the space between P^+ shoulders will be depleted essentially because of the lateral P^+N^- junction's built-in electric field. Therefore, the electron energy in the space is higher than that in the undepleted N^- and N region [as shown in Fig. 1(b)], which results in the hole potential well. Comparing the present structure with a conventional 4H-SiC APD, a greater reverse bias voltage will be needed to energize the holes through the potential well and into the high field region where they can undergo impact ionization. The hole potential well will suppress the avalanche of device and increase the V_{br}. The depth of the hole potential well will increase with the electric field intensity of lateral P^+N^- junction, enhancing the avalanche suppression effect and leading to a higher V_{br}.

The illumination-dependent V_{br} characteristic of the 4H-SiC NAPD can be explained as follows: the photon-generated carrier pairs partially negate the depletion of the open circuit P^+N^- junctions such that the total field intensity and potential well depth [as shown in Fig. 1(c)] change sufficiently to allow carriers to enter the high electric field region (n-type pillar) under a lower operation voltage. Under the condition of the same illumination power density, the numbers of photon-generated carriers are different at various illumination wavelengths, for the different photon energies and different absorption indeces. The numbers of the photon-generated carrier pairs will determine the variation range of the total field intensity and the potential well depth, which will cause a wavelength dependence of breakdown, while the illumination power density is a constant. More photon-generated hole-electron pairs will lead to a smaller electric field intensity of the P^+N^- junction. Then, a lower depth of the potential well and a smaller V_{br} will be achieved. Therefore, for 4H-SiC, while the illuminaiton power density is a constant for all the wavelength, there will be more hole- electron pairs at 280 nm than any other wavelength, corresponding to a minmum value of V_{br} for the 4H-SiC NAPD. In the same way, higher illumination power density will cause a higher photovoltaic filed and a smaller V_{br}, as shown in the Fig. 2 inset.

Due to the illumination-dependent V_{br}, avalanche self-quenching can be achieved for the 4H-SiC NAPD. Figure 3 shows the reverse I-V characteristics of the 4H-SiC NAPD with and without illumination. The wavelength and power density of the illumination are 280 nm and 1×10^{-4} W/cm^2, respectively. It is noted that the avalanche voltage (V_{br1}) of the 4H-SiC NAPD without illumination is higher than that (V_{br2}) with illumination, which is identical to the results in Fig. 2. Provided the operation voltage is set as the value of V_{br2}, the avalanche breakdown will be initiated for the 4H-SiC NAPD under 1×10^{-4} W/cm^2 illumination at λ of 280 nm. After removing the illumination, the avalanche voltage of the device changes to V_{br1}. Under the unilluminated condition, the breakdown voltage of NAPD (V_{br1}) is higher than the present operating voltage so the avalanche breakdown inside the device will quench automatically and the

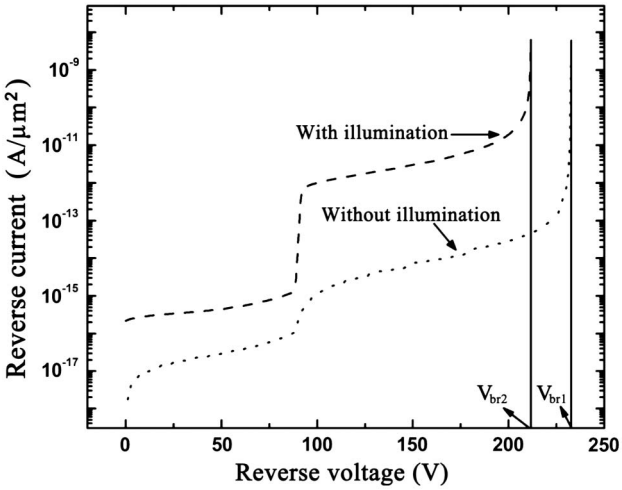

Fig. 3. Reverse I-V characteristics of the 4H-SiC NAPD with and without illumination. The wavelength and power density of the illumination are 280 nm and 1×10^{-4} W/cm^2, respectively.

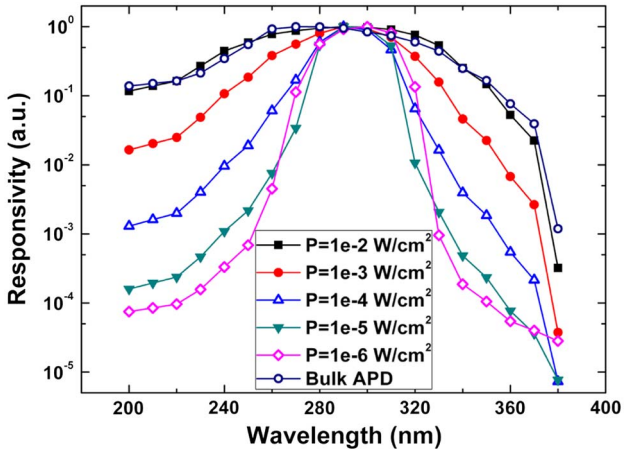

Fig. 4. (Color online) Normalized spectral responsivity of the 4H-SiC NAPD as a function of wavelength where the device is illuminated by a range of optical power densities and a comparison with a conventional bulk 4H-SiC APD.

photocurrent of the device will drop significantly. The self-quenching property of the 4H-SiC NAPD exists under any illumation condition, as the avalanche voltage of the 4H-SiC NAPD without illumination is always higher than that with illumiantion, as shown in Fig. 2. The self-quenching property of the NAPD can avoid the device operating in a broken-down state unnecessarily. The operation voltage would be set as the value V_{br2}; then, the NAPD is broken down only when optical illumination is incident into the device. Therefore, the lifetime of the device could be prolonged.

The illumination-dependent V_{br} can also lead to an ultrahigh UV/visible rejection ratio. Figure 4 shows the normalized spectral responsivity of the 4H-SiC NAPD as a function of wavelength where the device is illuminated by a range of optical power densities. Figure 4 also shows a comparison with a conventional bulk 4H-SiC APD. The bias of 4H-SiC NAPD is the V_{br} (corresponding to 1.0×10^{-7} A/μm reverse current) of the device under illumination with λ 280 nm and a specific illumination power density. It is noted that the 4H-SiC NAPD has an ultrahigh UV/visible rejection ratio, which can be explained by the illumination-dependent V_{br} property (as shown in Fig. 2) of the device. In Fig. 4, the 4H-SiC NAPD is in avalanche breakdown at 280 nm. However, there is no avalanche breakdown in the device at 380 nm. The photocurrent of the 4H-SiC NAPD with λ 280 nm will be significantly higher than that of 380 nm, leading to an ultra-high UV/visible rejection ratio. Comparing the UV/visible rejection ratio of the proposed device ($\sim 3.0 \times 10^3 - 1.3 \times 10^5$) to a bulk 4H-SiC APD ($\sim 8.4 \times 10^2$), the 4H-SiC NAPD exhibits an increase in rejection ratio between one and three orders of magnitude at the response peak, and a sharper decrease in responsivity away from the peak.

In conclusion, we have proposed a 4H-SiC NAPD featuring a nanoscale multiplication region separated from a larger bulk absorption region. The band structure, avalanche breakdown voltage, and photoresponse of the 4H-SiC NAPD are strongly dependent on illumination wavelength and power density. This novel device has the significant properties of self-quenching and ultrahigh UV/visible rejection ratio.

This work was partly supported by the National Natural Science Foundation of China (grant No. 61176049) and the Natural Science Foundation of Fujian Province (grant No. 2009J05151).

References

1. F. Yan, Y. Luo, J. H. Zhao, and G. H. Olsen, Electron Lett. **35**, 929 (1999).
2. H.-Ying Lee, H.-Lin Huang, and C.-Ting Lee, IEEE Photon. Technol. Lett. **23**, 706 (2011).
3. M.-L. Lee, T. S. Mue, F. W. Huang, J. H. Yang, and J. K. Sheu, Opt. Express **19**, 12658 (2011).
4. X. Kong, C. Liu, W. Dong, X. Zhang, C. Tao, L. Shen, J. Zhou, Y. Fei, and S. Ruan, Appl. Phys. Lett. **94**, 123502 (2009).
5. R. Yan, D. Gargas, and P. Yang, Nature Photon. **3**, 569 (2009).
6. H. Kind, H. Yan, B. Messer, M. Law, and P. Yang, Adv. Mater. **14**, 158 (2002).
7. Y. Han, G. Wu, H. Li, M. Wang, and H. Chen, Nanotechnology **21**, 185708 (2010).
8. O. Hayden, R. Agarwal, and C. M. Lieber, Nature Mater. **5**, 352 (2006).
9. M. Razeghi and A. Rogalski, J. Appl. Phys. **79**, 7433 (1996).
10. X. Guo, A. L. Beck, Z. Huang, N. Duan, J. C. Campbell, D. Emerson, and J. J. Sumakeris, IEEE Trans. Electron Devices **53**, 2259 (2006).
11. X. Zhang, P. Kung, D. Walker, J. Piotrowski, A. Rogalski, A. Saxler, and M. Razeghi, Appl. Phys. Lett. **67**, 2028 (1995).
12. M. Razeghi, Proc. IEEE **90**, 1006 (2002).
13. A. Vert, S. Soloviev, and P. Sandvik, Mater. Sci. Forum **645–648**, 1069 (2010).
14. X. Guo, A. Beck, Z. Huang, N. Duan, J. Campbell, D. Emerson, and J. Sumakeris, IEEE Trans. Electron Devices **53**, 2259 (2006).
15. W. Loh, B. Ng, J. Ng, S. Soloviev, H.-Y. Cha, P. Sandvik, C. John-son, and J. David, IEEE Trans. Electron Devices **55**, 1984 (2008).
16. K. Li, H. Liu, Q. Zhou, D. Mcintosh, and J. C. Campbell, Opt. Express **18**, 11713 (2010).
17. H. Cha and P. M. Sandvik, Jpn. J. Appl. Phys. **47**, 5423 (2008).